Journal of Materials Chemistry C

Accepted Manuscript

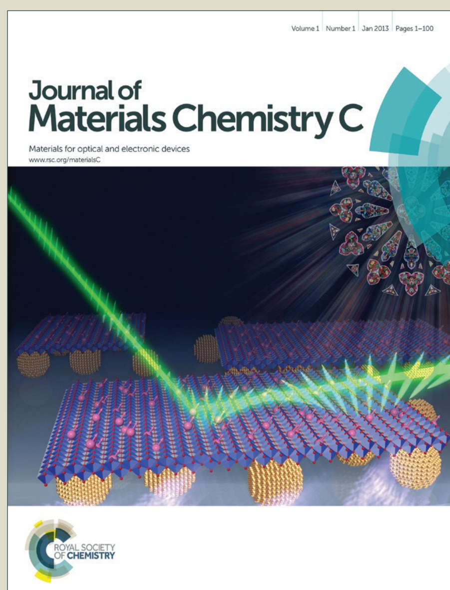

This is an *Accepted Manuscript*, which has been through the Royal Society of Chemistry peer review process and has been accepted for publication.

Accepted Manuscripts are published online shortly after acceptance, before technical editing, formatting and proof reading. Using this free service, authors can make their results available to the community, in citable form, before we publish the edited article. We will replace this *Accepted Manuscript* with the edited and formatted *Advance Article* as soon as it is available.

You can find more information about *Accepted Manuscripts* in the Information for Authors.

Please note that technical editing may introduce minor changes to the text and/or graphics, which may alter content. The journal's standard Terms & Conditions and the Ethical guidelines still apply. In no event shall the Royal Society of Chemistry be held responsible for any errors or omissions in this *Accepted Manuscript* or any consequences arising from the use of any information it contains.

ROYAL SOCIETY OF CHEMISTRY

www.rsc.org/materialsC

Please do not adjust margins

Journal Name

ARTICLE

Effects of Proton Irradiation on Si-Nanocrystal/SiO_2 Multilayers: Study of Photoluminescence and First-Principles Calculation†

Received 00th June 2015, Accepted 00th July 2015

DOI: 10.1039/x0xx00000x

www.rsc.org/

Seunghun Jang,[a,c] Beom Soo Joo,[a] Sung Kim,[b] Ki-jeong Kong,[c] Hyunju Chang,[c] Byung Deok Yu[a] and Moonsup Han*[a]

Si nanocrystal (NC)/SiO_2 multilayers containing interfacial nitrogens are formed by radiofrequency magnetron-sputtering and post-annealing. Analyzing the photoluminescence (PL) of the multilayer structures after proton irradiation (PI), we found that the peak at ~740 nm was shifted toward shorter wavelengths and that its intensity was considerably suppressed. Furthermore, a new peak simultaneously appeared at ~500 nm. We interpret that PI not only modifies the shapes of the Si NCs and generate defects at the NC/SiO_2 interface, but also induces simultaneously hydrogen passivation (HP) of interfacial nitrogens due to the attenuated protons. To investigate the relation between the HP of N at a Si NC/SiO_2 interface and the observed band gap reduction of Si NC structures within the SiO_2 matrix, we modeled the atomic configurations at the interface and applied a first-principles calculation. The results clearly indicate that the HP of composite structures containing Si-N bonds at the Si NC/SiO_2 interface induces the blue-shift in PL. We expect that this investigation helps to pave a way to develop more efficiently Si-based light emitting devices or solar cells technologies.

Introduction

Since the discovery of strong light emission in the red wavelength region from porous Si,[1] the optical properties of Si nanostructures (NSs) have been investigated intensively by many researchers over the last two decades owing to their enormous potential for application in Si-based optoelectronic devices,[2] light-emitting diodes (LEDs),[3-5] and third-generation photovoltaics.[6] Especially, the external quantum efficiencies of Si-NS based LEDs have been steadily studied.[7-9] Among the various investigations of Si NSs, Si nanocrystals (NCs) embedded in SiO_2 matrices built in the form of periodic multilayers have been studied because of their superior properties, such as ease of NC size control and strong luminescence.[10-11]

The mechanisms of light emission from a Si NC/SiO_2 system have been explained by many groups. Light emission from Si NCs has been attributed to the size-dependent quantum-confinement effect (QCE);[10-14] The Si=O surface state of porous Si quantum dots (d < 3 nm) plays an crucial role to form recombination between trapped excitons;[15] PL quenching behaviour resulting from controlling the Si NC/SiO_2 interfacial states has been ascribed to localized defects;[16] and defect formation in SiO_2 accompanies a new emission peak centered at ~500 nm.[17-19] In particular, numerous studies of the electronic and optical properties of the atomic bonding configurations at a Si NC/SiO_2 interface are now in progress.[20,21] However, these studies have focused only on one individual region among all the relevant ones such as SiO_2 matrices, NC cores, and NC/SiO_2 interfaces to the luminescence. In order to achieve a more complete understanding, it is essential to investigate the interrelation between all the relevant regions of a Si NC/SiO_2 system.

Furthermore, studies on freestanding Si NC that is not surrounded by a SiO_2 host matrix have recently begun. According to Dasog *et al.*, without changing the Si NC size, the PL of Si NCs could vary based on the surface functionalization.[22,23] Depending on the functional group used in surface passivation, the peak PL position from functionalized Si NC changes in the visible wavelength range, which suggests that the size-independent interface-reaction dynamics, as well as NC size control, are key to the utilization of Si NCs for future optical devices and photovoltaics. Accordingly, to optimize the quantum efficiency and emission range from Si NCs, it is important to engineer the passivation configuration at a Si NC surface and to understand the interrelation between interfacial state formation and optical transition from the electronic structure of NCs imbedded in an oxide matrix.

In order to adequately address these requirements of Si NC/SiO_2 systems, we utilized proton irradiation (PI) to modify the nanostructured multilayers as mentioned, as this method could efficiently affect controlled changes in each relevant region and systematically investigate the effects of these changes on various luminescent properties.[24,25] Since protons

[a]Department of Physics, University of Seoul, Seoul, 130-743, Republic of Korea. E-mail: mhan@uos.ac.kr; Fax: +82-2-6490-2644; Tel: +82-2-6490-2647
[b]Department of Applied Physics, College of Applied Science, Kyung Hee University, Yongin 446-701, Republic of Korea
[c]Present address: Advanced Materials Division, Korea Research Institute of Chemical Technology (KRICT), Daejeon, 305-343, Republic of Korea
† Electronic Supplementary Information (ESI) available. See DOI: 10.1039/x0xx00000x

Journal of Materials Chemistry C Accepted Manuscript

Please do not adjust margins

have the smallest atomic mass, we anticipate modest structural modification requirements for such samples as compared to those for other massive ions. Furthermore, PI essentially replaces H implantation because it causes hydrogen passivation (HP) at the NC/SiO_2 interface, which stabilizes NC structures on the atomic level.

All of the above-mentioned factors could modify the spectral weight and range of PL in the investigated samples. If we could select and tune the emission wavelength, it would be more useful to generate shorter wavelengths for full-color LED applications and/or efficient energy harvesting with the above-mentioned Si-based NSs. Therefore, we are actively working towards identifying an efficient fabrication process to engineer multi-layered Si NC/SiO_2 systems that emit wavelengths below 600 nm by understanding the luminescence mechanism in this spectral range.

In this investigation, we studied the changes in PL of Si NC/SiO_2 multilayers induced by PI, which readily controls not only the shape and size of NCs but also size-independent factors, such as the various defects in a SiO_2 matrix or at a Si NC/SiO_2 interface. We also investigated the influence of the atomic bonding configurations at the Si NC/SiO_2 interface on the PL spectrum by using an ab initio density-functional-theory (DFT) calculation. The appropriate model and results of the calculation for NS systems with intricate interfaces at the atomic level could be essential in understanding the luminescence mechanism and achieving an efficient method of selecting and tuning the emission wavelengths of Si-based NS systems.

Experimental

Sample Preparation

A multilayer consisting of 20 SiO_x/SiO_2 bilayer stacks was deposited on a 2 in p-type (100)-Si wafer by alternate RF-magnetron sputtering under an Ar or O_2 atmosphere. Si single crystals with a purity of 5N (99.999%) were used as the sputtering targets. The SiO_x and SiO_2 layer thicknesses were 3 nm and 4 nm, respectively. Subsequently, a 10 nm SiO_2 capping layer was deposited on the multilayer stack to prevent unintended oxidation of the uppermost Si NC layer during the post-annealing process. To obtain homogeneous films, the wafer was always rotated during the sputtered deposition. In order to form Si NCs in the SiO_x layer, the thermal annealing processes were conducted in a quartz-tube furnace (1100 ˚C, 1 h) under an N_2 atmosphere.

Proton Irradiation (PI)

In order to generate luminescent defects and investigate luminescent origins, we performed PI of Si NC/SiO_2 multilayer samples using a MC-50 cyclotron at the Korea Institute of Radiological and Medical Sciences at RT and under a medium vacuum atmosphere. The proton beam energy decreased from 20 MeV initially to 3.5 MeV by passing through Al degraders. The proton beam direction was perpendicular to the plane of the Si NC/SiO_2 multilayer. In our study, the total fluences during PI at an energy of 3.5 MeV were 1×10^{13} cm^{-2}, 5×10^{14} cm^{-2}, and 1×10^{15} cm^{-2}, and the irradiation times corresponding to each fluence were 50 s, 2500 s, and 5000 s (see Figure S5).

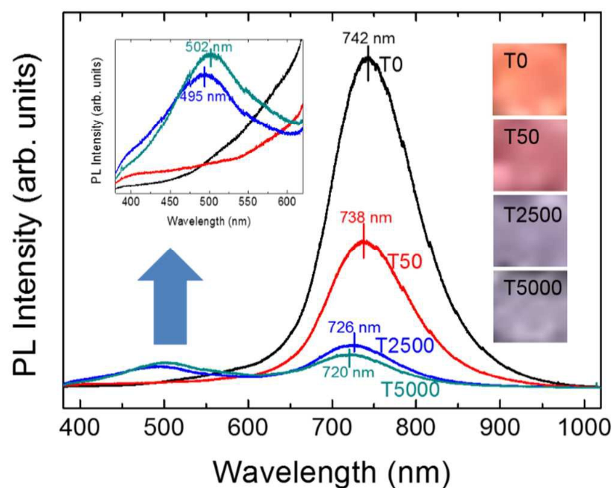

Figure 1. (Color online) PL spectra (middle) and photographs (right) for the T0 (as-crystallized), T50, T2500, and T5000 samples.

PL and TR-PL Measurements

PL spectra at room temperature were obtained by using a HORIBA®'s PL spectrometer (Fluorolog®-3) with a He–Cd laser (325 nm, 25 mW). The excitation for TR-PL was performed by an optical parametric oscillator pumped by a pulsed Nd:YAG laser (wavelength: 355 nm, pulse energy density: 0.6 mJ/cm^2, repetition frequency: 20 Hz, and pulse duration: 20 ps). The emitted light was analysed by using a monochromator equipped with a gated ICCD (detection energy: 1.38–9.92 eV, response time: 40 ps, PIMax, Princeton Instrument) triggered by an exciting laser pulse.

TEM and FTIR Measurements

Bright-field TEM cross-section micrographs were taken with a JEM-ARM 200F operated at 200 kV. HRTEM was used to study the microstructural properties of the materials. FT-IR spectroscopy (Bruker IFS 66v/s) was performed to examine the effects of PI on various vibrational bonds in the Si NC/SiO_2 multilayer under the attenuated total reflection mode.

RESULTS AND DISCUSSION

Proton-irradiation-induced spectral change in NC/SiO_2 multilayer

We observed a cross-sectional TEM image of the Si NC/SiO_2 multilayer sample in the crystallized state after annealing at 1100 °C (see Figure S1). A Si NC/SiO_2 multilayer structure contains 20 Si NC layers. The periodic Si NC structure perpendicular to the substrate plane was clearly identified. The average diameter and areal density of the Si NCs were estimated to be about 3–4 nm and 6.9×10^{11} cm^{-2},

Journal of Materials Chemistry C Accepted Manuscript

This journal is © The Royal Society of Chemistry 20xx

Please do not adjust margins

respectively. Detailed analysis of the Si NCs will follow later in this section.

Figure 1 shows the PL spectra (middle) and photographs (right) for the T0 (as-crystallized), T50, T2500, and T5000 samples. The samples are labelled by the PI duration time (e.g., the sample with 2500 s PI time is labelled T2500, etc.). From the PL spectra, we can identify three main features. First, the peak position at ~740 nm is shifted toward shorter wavelengths as the PI time increases. Second, the PL intensity due to Si NCs decreases as the proton dose increases. Finally, a new peak at ~500 nm emerges when the appropriate irradiation time is reached. These features can also be observed from the color change in the photographs in the column on the right side of the figure. The left inset shows the development of the PL at ~500 nm. In order to systematically investigate the spectral developments in PL of NC/SiO_2 by PI, we divided the investigated sample area into four individual regions: the Si substrate, SiO_2 matrix, Si NCs, and Si NC/SiO_2 interface. We will discuss the interrelation between the changes in each region resulting from PI and the luminescence behaviour of the sample.

Proton-irradiated Si substrate

We estimated the total thickness of the Si NC/SiO_2 multilayer to be ~160 nm based on the cross-sectional TEM image. Since the penetration depth of an incident proton from a beam with an energy of 3.5 MeV is longer than 100 μm, most incident protons reach the Si substrate through the Si NC/SiO_2 multilayer.[26] Thus, we investigated the influence of PI on the Si substrate. A bare p-Si wafer (100) was subjected to a proton beam with 3.5 MeV energy and a flux of 1×10^{15} protons/cm^2. However, we could not observe any PL signal from the proton-irradiated Si wafer. Therefore, we excluded the possibility that a Si substrate under a proton-irradiated NC/SiO_2 multilayer affects the changes in the PL spectra.

Proton-irradiated SiO_2 matrix

Next, we investigated the SiO_2 matrix as a potential cause of the PL changes. In order to investigate this possibility in more detail, a pure SiO_2 layer with 20 nm thickness was deposited on a Si substrate. We measured the PL spectra of the SiO_2 film after PI and found that the PL emission at ~500 nm from the SiO_2 film appeared despite the absence of Si NC (see Figure S2). This result indicates that the PL peak at ~500 nm shown in Figure 1 should be mainly attributed to defects in proton-irradiated SiO_2 matrix but not to defects in Si NCs region. Previous studies have well explained the emission at ~500 nm from pure SiO_2 by self-trapped excitons (STEs).[17,18,27,28] We expect that PI could generate excited electrons and holes throughout the SiO_2 matrix, so an electron-hole pair (exciton) could subsequently be formed and induce localized lattice distortions. In other words, the exciton traps itself at a distortion site to lower the total energy of the local atomic environment.[27] We note that the STEs formed by this process in SiO_2 film lead to defects such as an E' center and a non-bridging oxygen hole center (NBOHC).[27] Furthermore, some investigations that pulsed electron irradiation onto amorphous SiO_2 thin films resulted in light emission at ~515 nm.[29,30] Accordingly, we are convinced that the luminescence at ~500 nm can be attributed to the radiative recombination of STEs caused by PI in the amorphous SiO_2 matrix region in the sample.

This STE model in amorphous SiO_2 is further supported by PL data for hydrogen-gas annealing at 400 °C for 30 min in proton-irradiated SiO_2 film. We confirmed that the PL peak at ~500 nm disappeared completely after hydrogen-gas annealing (see Figure S2). This result indicates that defects, such as an E' center or a NBOHC, are readily passivated by H and transformed into non-radiative centers following H_2 annealing.

Proton-irradiated Si NCs

Prior to or after PI, it is necessary to track the changes in the luminescent properties originating from the Si NC region. We compared the microscopic and structural characteristics of the

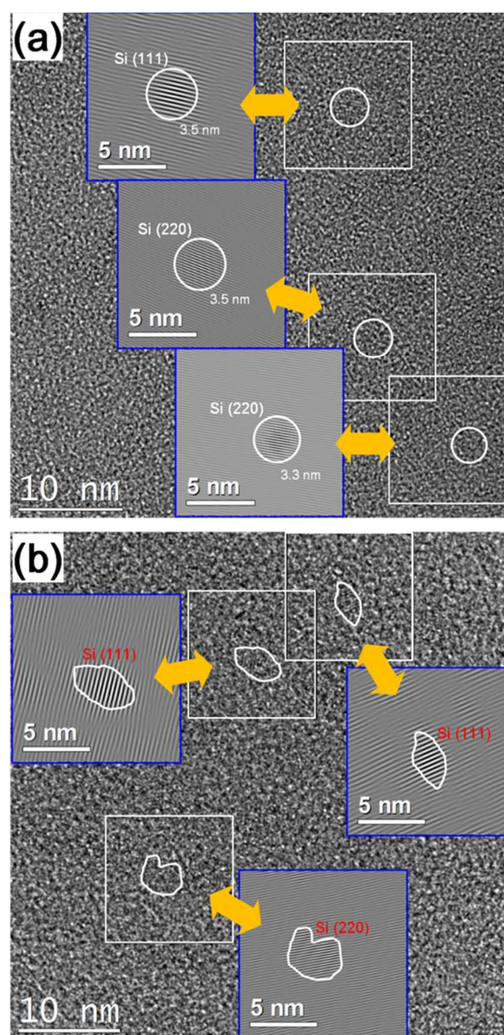

Figure 2. HRTEM image (white box) and Bragg-filtered HRTEM image (blue box) for three Si NCs in regions of the (a) T0 and (b) T5000 samples.

Journal of Materials Chemistry C Accepted Manuscript

Please do not adjust margins

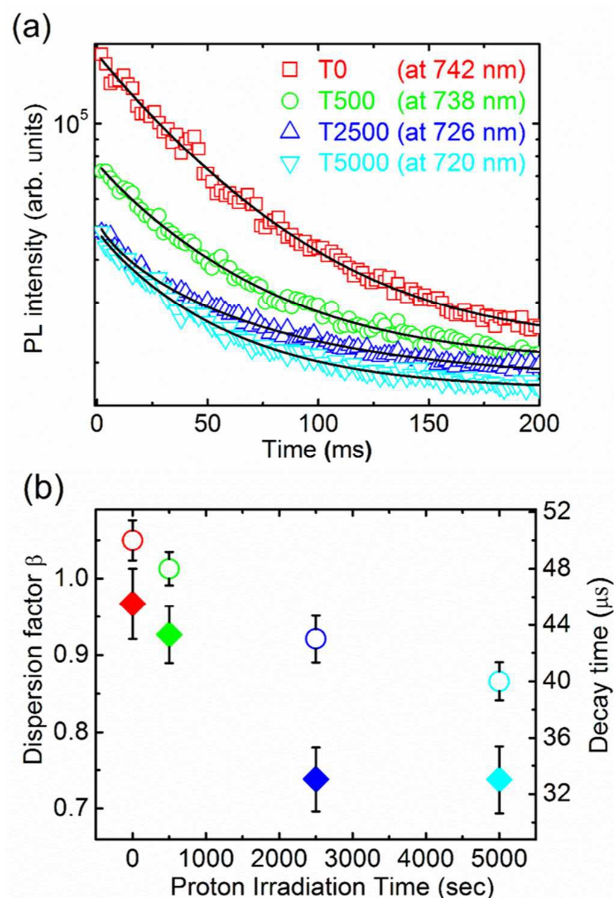

Figure 3. (a) PL decay of samples T0, T500, T2500, and T5000. The black lines are the stretched exponential fits. The results of all stretched exponential fits of sample set T are given below: (b) dispersion factor β (filled diamond) and luminescence lifetime τ (open circle) of the proton irradiation.

T0 and T5000 samples by high-resolution TEM (HRTEM). Figure 2 shows cross-sectional and Bragg-filtered HRTEM images for the T0 and T5000 samples, which contained Si NCs. The Bragg-filtered HRTEM images were pre-processed by the FFT filtering method (see Figure S3). In the HRTEM images for both T0 and T5000, three different NC regions were selected. All NCs exhibit spherical shapes with diameters of ~3.5 nm, as shown in Figure 2a. In addition, the d-spacing between the fringes of the selected Si NCs corresponds with that of the Si (220) or Si (110) plane. On the other hand, the NCs in T5000 predominantly exhibit not only non-spherical shapes but also smaller sizes, as shown in right column of Figure 2b. However, the fringes in the NC core were maintained even after PI.

In order to analyse the changes in the PL decay characteristics upon PI, we performed time-resolved PL (TRPL) at the peak wavelength of each sample, as shown in Figure 3. The PL decay data were fitted by the stretched exponential function

$$I(t) = I_0 \exp\left[-(t/\tau)^{\beta}\right],$$

which is well known to researchers.[16] Figure 3b presents the behaviour of the decay time τ and dispersion factor β upon PI. It can be seen that τ decreases as the PI time increases. Two points can be inferred from these results. The first concerns NC size reduction. Previous studies have reported that with decreasing NC size, τ tends to decrease because the required phonon contribution to the luminescence decay of an exciton decreases.[20,31] Thus, the change in τ indicates that the NC size decreases due to PI. This result is consistent with the observed NC size reduction in Figure 2. Thus, it explains why the PL peak at ~740 nm is blue-shifted to shorter wavelengths with increasing PI flux, as shown in Figure 1.

The second point is linked to the interfacial defects. There are literatures that τ became shorter by increasing the amount of NC/SiO_2 interfacial defects during annealing process.[16,20,32] Meanwhile, β becomes smaller with increasing PI time. These investigations have correlated β decrease to generation of NC/SiO_2 interfacial defects and NC size broadening.[16,20,32-34] Thus, we interpret that the PI induces a number of NC/SiO_2 interfacial defects as well as extends size distribution of NCs, which causes to notable suppression of the PL from the NCs.

HP at NC/SiO_2 interface

In addition, it is important to investigate the influence of HP by the remaining protons in the NC/SiO_2 multilayer. Thus, it was necessary to obtain information about the final locations of the protons that affected the SiO_2 matrix and Si NCs. To obtain this information, an FTIR experiment was performed. Figure 4 shows the FTIR spectra for the proton-irradiated NC/SiO_2 multilayer. The FTIR data exhibits typical SiO_2 features, including the Si-O-Si stretching band at 1045-1075 cm^{-1} and Si-O-Si bending mode at 810 cm^{-1}. Interestingly, we observe the Si-N peak at 960 cm^{-1} and Si-NH bending vibration mode at 1120-1180 cm^{-1}. The absorption peak corresponding to SiO_2 diminishes with increasing PI flux, as expected from the results shown in Figure 1. However, the peak corresponding to the Si-NH bending vibration mode increases. According to Ref. 20, a NC/SiO_2 multilayer annealed in a N_2 gas atmosphere has Si-N

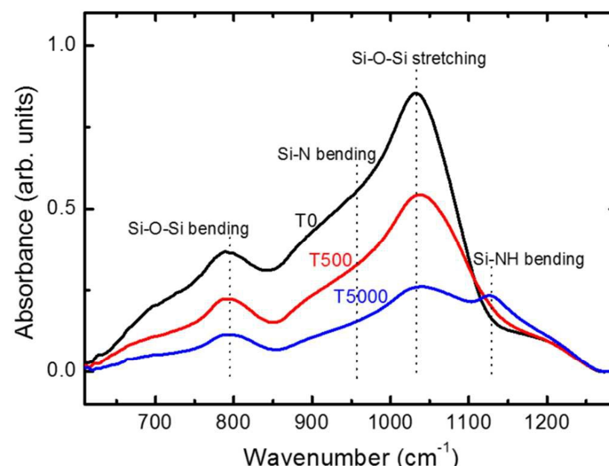

Figure 4. FTIR spectra of the proton-irradiated Si NC/SiO_2 multilayer.

This journal is © The Royal Society of Chemistry 20xx

Journal of Materials Chemistry C Accepted Manuscript

Please do not adjust margins

bonds at the interface between the NCs and SiO_2 matrix. This feature implies that the Si-NH bending vibration mode in the FTIR results originates from the NC/SiO_2 interface. Thus, we can conclude that the protons that affected the SiO_2 matrix and NC are finally located at the Si NC/SiO_2 interface, which suggests the HP of N atoms with dangling bonds at the interface due to the energy-attenuated protons. Furthermore, it should be noted that the peak corresponding to the Si-N bending vibration mode has decreased, which indicates that a considerable number of protons contribute to breaking Si-N bonds and subsequently forming Si-NH bonds at the Si NC/SiO_2 interface.

HP effect versus NC size effect

Now, we turn to understanding the interrelation between the luminescence and increase in the number of Si-NH bonds at the NC/SiO_2 interface. Recently, Hiller *et al.* suggested that the blue-shift of the PL from N_2-annealed NC/SiO_2 compared to the PL from Ar-annealed NC/SiO_2 is based on an increased NC band gap that results from interfacial N.[20] That suggestion implies that the blue-shift of the PL from NCs in Figure 1 is associated with the passivation of interfacial H from Si-N bonds to Si-NH bonds at the NC/SiO_2 interface. To confirm this possibility, additional annealing was performed under H_2 for the T5000 sample. As a result, the emission peak at ~500 nm was almost completely suppressed, whereas the PL peak at ~720 nm was somewhat shifted toward longer wavelengths (see Figure S4). In other words, for the composite structure containing Si-N bonds at the NC/SiO_2 interface, additional H_2 gas annealing after the PI leads to a red-shift of the NC-related PL peak, while the chemical reaction of HP due to the PI itself causes a blue-shift of the peak, as shown in Figure 1.

In order to investigate the influence of HP due to the PI on the NC electronic structure at a NC/SiO_2 interface containing Si-N bonds, it is necessary to conduct an appropriate simulation for a composite structure that contains Si-N bonds residing at the Si NC/SiO_2 interface. A theoretical approach using ab initio DFT calculations can be effective to investigate the geometric and electronic changes at the microscopic level, such as those at a Si NC/SiO_2 interface.

MD and DFT calculations for model configurations at Si NC/SiO_2 interfaces

First-principles calculations were performed using DFT implemented in the Vienna Ab-initio Simulation Package (VASP) code.[35,36] The exchange–correlation functional was approximated with the Perdew–Burke–Ernzerhof (PBE) expression.[37] For electron-ion interactions, the projector-augmented wave (PAW) method was used.[38] The electronic wave functions were expanded in a basis set of plane waves with a kinetic energy cutoff of 400 eV. To optimize the geometry, Brillouin-zone (BZ) integrations were carried out using only the Γ point. To calculate the density of states, on the other hand, the k-space integration was performed with a finite sampling of selected k points on a 2×2×2 mesh in the BZ that were generated according to the Monkhorst–Pack scheme.

In this model calculation, we considered the three most significant geometries of Si NCs, specifically those passivated by H, N, and NH at the interface, as shown in the green circles of Figures 5a-c. An H-passivated Si NC represents a Si NC/SiO_2 interface with only one Si-H bond, and an N-passivated Si NC represents an interface with one Si-N bond. The NH-passivated Si NC was designed to consider an interface containing one Si-NH and one Si-H bond. Si NCs with fixed 1.1 nm diameters were considered in all geometries of the model calculation to reduce computation. We will focus on and discuss the relative changes of the electronic structures of these specific atomic configurations at the NC/SiO_2 interface due to the inevitable differences between the experiment and model calculations.

Generation of atomic geometry

The atomic structure was generated by combining classical molecular dynamics (MD) simulations and the DFT method. We began with a β-cristobalite cell containing 432 O atoms and 216 Si atoms. To generate a realistic amorphous SiO_2 matrix, classical MD simulations were conducted using Tersoff interatomic potentials implemented in LAMMPS code. This initial geometry was amorphized by annealing at a temperature of 4000 K for 100 ps and quenching at a rate of 100 K/ps down to 300 K. Then it was optimized through MD simulations.[39] After the amorphization process for oxide, we removed all atoms in a given 1.1 nm diameter sphere and filled it with Si NCs. The final atomic geometry of the Si NC/SiO_2 was obtained by performing additional first-principles calculations to optimize all the ionic coordinates. Geometric optimization was performed until the residual forces decreased to below 0.05 eV/Å. In order to eliminate the effects of unsaturated bonds at the interface and in the matrix, we added a few H atoms to the system.

Density of states and energy gaps for model configurations

Figure 5 depicts the relaxed atomic geometries and electronic density of states (EDOS) of Si NCs passivated by different atomic configurations at the Si NC/a-SiO_2 interface. The atomic geometry in Figure 5a was generated using the procedure described above. As a result, at the Si NC/a-SiO_2 interface, there existed one H atom to passivate a Si dangling bond. On the other hand, a Si-N bond at the Si NC/SiO_2 interface was produced by replacing one H and its bonded Si on the NC surface with one N atom, as shown in Figure 5b. Furthermore, N-H bonds at the Si NC/a-SiO_2 interface were constructed by performing HP on broken Si-N bonds. All geometries were obtained through complete ionic relaxation.

To investigate the relation between the electronic structure and atomic configuration of the interfacial region in the Si NC/a-SiO_2, we calculated the EDOS. As a result, the change in the Si NC band gap in the passivation configuration was observed. The band gap energies of H-passivated, N-passivated, and NH-passivated Si NCs were 1.06 eV, 1.11 eV, and 1.19 eV, respectively. To ensure reliability on the tendency

Journal of Materials Chemistry C Accepted Manuscript

Please do not adjust margins

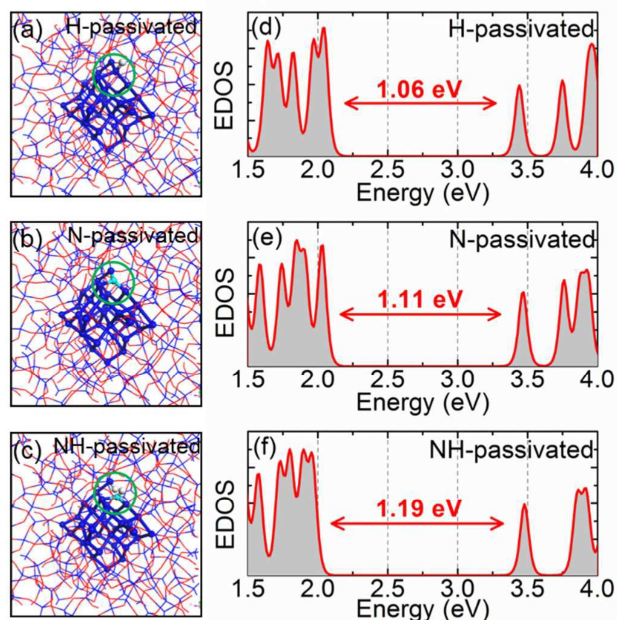

Figure 5. (Color online) Calculated atomic geometries and EDOS of Si NCs passivated by different atomic configurations at Si NC/a-SiO_2 interface. (a), (b) H-passivated Si NC; (c), (d) N-passivated Si NC; (e), (f) NH-passivated Si NC. The Si, N, and H atoms in the core are represented by dark blue, light blue, and white balls, respectively, and Si-O bonds in the matrix are represented by solid lines.

of band gap that we calculate, it is thought that it needs to perform more exact calculations. Considering computational resources in general, however, advanced calculations such as hybrid functional DFT study have size limits on number of atoms. Surveying broadly DFT hybrid functional studied on various silicon related materials, we confirmed that the tendencies of band gap estimation by PBE level has been in parallel to those by hybrid functional.[40-42] We expect in our model study that the PBE level discussion for three relevant configurations as shown in Figure 5 would not be far from a hybrid functional one.

According to a previous DFT calculation study on H-passivated Si NC, the H-passivated NC structure had a higher band gap than did the oxide-passivated one.[43] However, the structure used in Ref. 43 had no surrounding a-SiO_2 matrix. Since the electronic structure of Si NCs embedded in an a-SiO_2 matrix is expected to be severely affected by the strain at the interface between the NC core and a-SiO_2 matrix,[21] it may be not appropriate to apply the DFT calculation to the Si NCs without considering the strain effect. The calculation in this work produced strain relaxation at the interface and applied realistic HP at the NC/SiO_2 interface with Si-N bonds, which could help to more accurately understand the electronic properties of the samples annealed under a N_2 gas atmosphere in this work.

From our calculations, we observed that the band gap of a NC with a Si-N bond at the Si NC/a-SiO_2 interface is wider than that for a NC with a Si-H bond. We also found that the band gap increased when a Si-N bond was broken and formed into a Si-NH or Si-H bond by HP. These results answer the question presented in Section 2.5. The HP for a composite structure including Si-N bonds at the Si NC/a-SiO_2 interface seems to widen the Si NC band gap, which explains the blue-shift in the PL spectrum. Thus, if we consider the increase in the Si-NH bending mode by PI that is demonstrated by the FTIR results, we can conclude that blue-shift of the ~740 nm PL peak by the PI may be ascribed not only to size-dependent factors, such as the reduction and deformation of Si NCs, but also to size-independent factors, such as the active H reaction at the NC/a-SiO_2 interface with a Si-N bond.

Origin of band gap change based on model study

Let us closely examine the band gap change of the local atomic configuration at the surface of a 1.1 nm diameter Si NC, as shown in Figures 6a-c. The band gap of the total Si NC/SiO_2 system can be controlled by changing just one specific configuration. In our model, we dealt with only one local atomic configuration in one unit cell. However, a real Si NC/SiO_2 system will include numerous atomic configurations at its interface, such as Si-H, Si-N, and S-NH. Thus, we expect that the band gap of real Si NC/SiO_2 will be sensitive to the specific types of atomic bonds at its interface.

In order to study the origin of the band gap change for

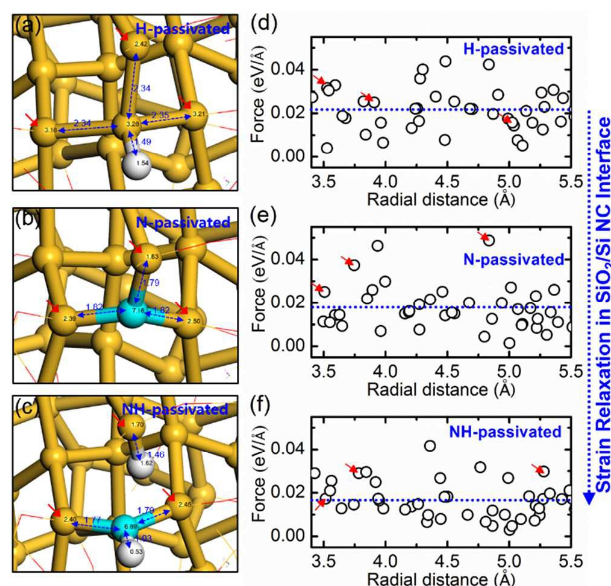

Figure 6. (Color online). Charge values in units of absolute electron charge (black numbers) and bond lengths (blue numbers) between passivated Si atoms and their nearest-neighbour atoms in the interfacial region: (a) H-passivated, (b) N-passivated, and (c) NH-passivated. Profiles of residual forces applied to all interfacial atoms with the following atomic configurations in the interface: (d) H-passivated, (e) N-passivated, and (f) NH-passivated. Three passivation-related Si atoms are indicated by the arrows for each interfacial configuration. The average strain relaxation is depicted by horizontal dotted lines in the right-hand figures.

This journal is © The Royal Society of Chemistry 20xx

Journal of Materials Chemistry C Accepted Manuscript

Please do not adjust margins

various local atomic configurations in Si NC/SiO_2, Bader charge and local structure analyses were performed. Figure 6 shows the charge values in units of absolute electron charge and the bond lengths between passivated Si atoms and their nearest-neighbour atoms in the interfacial region. In Figure 6a, the charge (black numbers) of the Si atom in Si NC was determined from the oxidation numbers. The charge of Si in a Si-H bond is similar to that of Si bonded with three Si atoms and one O. Meanwhile, when a Si-N bond is formed, the N atom brings more electrons from nearest-neighbour Si atoms than does the Si atom bonded with H in a H-passivated Si NC. This characteristic subsequently leads to bond-length shortening of the three Si-N bonds. The bond lengths (blue numbers) were 2.34 Å, 2.34 Å, and 2.35 Å for the three Si-Si bonds near the Si-H bond in Figure 6a. These lengths decreased to 1.79 Å, 1.82 Å, and 1.82 Å for the Si-N bonds in Figure 6b. This local structural change in the interfacial region might cause local strain between the NC core and SiO_2 matrix. On the other hand, in the model calculation for NH-passivated Si NC, a N atom bonded with two Si atoms and an H due to the two additional H atoms. This process was followed by breaking of the Si-N bond. In this case, the N atom bonded more strongly with the two Si atoms due to the electron-deficient atmosphere. According to Bader charge analysis, the polarities of Si-N bonds decrease compared to that of a Si-N bond in N-passivated Si NC, and two very short Si-N bonds are formed.

Now we investigate the profiles of the residual forces applied to all interfacial atoms with the following atomic configurations at the interface. The interfacial region is defined as a monolayer of Si atoms on a Si NC surface. We consider ~5.5 Å to be the distance from the NC center to the surface and 2 Å to be the thickness of the Si monolayer. These distances provide important information about how the local strain induced by interfacial chemical reactions influences the overall rearrangement of atoms in the interfacial region. Interestingly, the average forces (blue dotted horizontal lines) of atoms in the interfacial region all relaxed for the H-passivated, N-passivated, and NH-passivated Si NC/SiO_2 interfaces, as shown in Figures 6d-f. The images in Figure 6 depict the following: (i) At the H-passivated Si NC/SiO_2 interface, each of the three Si atoms (red arrows in Figures 6a and 6d) around the central Si that bonded with one H causes strain on the other interfacial atoms and resides at the interface. (ii) At the N-passivated Si NC/SiO_2 interface, strong strains are applied to the three Si atoms (red arrows in Figures 6b and 6e) near the N atom, while the average strains applied to the remaining Si atoms in the interfacial region decrease. (iii) At the NH-passivated Si NC/SiO_2 interface, the average strains on the interfacial Si atoms relax, while the Si-N bond is broken by the two additional H atoms. These results suggest that the average strain around Si atoms in an interfacial region could be controlled by altering the local atomic configuration. According to previous studies[21,44] on the relation between interfacial strain and band gap in a Si NC-related system, strain relaxation in an interfacial region enlarges the bandgap. From both the calculations and experimental results of this investigation, we can conclude that the sensitivity to atomic configuration rearrangements near interfacial Si atoms in an NC/SiO_2 interfacial region could play an important role in determining the band gap for Si NC-embedded NSs.

Conclusions

We investigated the origin of the PL change of Si NC/SiO_2 multilayers that is induced by PI. Analysing the PL, TEM, and TRPL results, we found that the blue-shift for the peak at ~740 nm is caused by the size reduction of Si NC by the PI as well as by the chemical reaction at the Si NC/SiO_2 interface. Furthermore, we found that the salient suppression of the PL at ~740 nm is associated with an increase in the interfacial defects. We determined that PI actively leads actively to HP of N-related dangling bonds at the interface via the energy-attenuated protons. The appearance of a new PL peak at ~500 nm in the proton-irradiated Si NC/SiO_2 multilayer was assigned to the radiative recombination of the STE in an irradiation-induced a-SiO_2 matrix.

We performed first-principles calculations for three different passivated configurations near an unpaired interfacial Si atom. The calculations clearly indicate that the HP for a composite structure containing Si-N bonds at the NC/SiO_2 interface induces a blue-shift in the PL. This result implies that the blue-shift of the PL peak at ~740 nm by the PI was driven not only by the reduction and deformation of Si NCs but also by the effects of HP at the NC/SiO_2 interface with a Si-N bond. In addition, we determined that the NH-passivated configuration at a Si NC/SiO_2 interface reduces the total strain in the interfacial region, which causes the band gap to widen. This result implies that the sensitivity to atomic configuration rearrangement near interfacial Si atoms in a NC/SiO_2 interfacial region could be important in determining the band gap of Si NC-imbedded NSs.

On the other hand, the experimental results as well as the calculations in this investigation indicate that PI is an effective way to control the structural and luminescent properties in all the relevant regions, including the NC core, host oxide, and interfacial regions, in Si NC/SiO_2 multilayers containing interfacial nitrogens. Therefore, these results are expected to prove useful in the systematic adjustment of optical and other related properties for the development of Si-based LEDs and solar cells.

Acknowledgements

We acknowledge support from the National Research Foundation of Korea under Grant Nos. NRF-2012M2B2A4029470 and NRF-2014M2B2A4031923.

Notes and references

1 L. T. Canham, *Appl. Phys. Lett.*, 1990, **57**, 1046.
2 L. T. Canham, *Nature*, 2000, **408**, 411.
3 L. Pavesi, L. D. Negro, C. Mazzoleni, G. Franzo and F. Priolo, *Nature*, 2000, **408**, 440.

Journal of Materials Chemistry C Accepted Manuscript

Please do not adjust margins

4 R. J. Walters, G. I. Bourianoff and H. A. Atwater, *Nat. Mater.*, 2005, **4**, 143.
5 S. Jang and M. Han, *J. Alloys Comp*. 2013, **614**, 102.
6 G. Conibeer, M. Green, R. Corkish, Y. Cho, E. C. Cho, C. W. Jiang, T. Fangsuwannarak, E. Pink, Y. Huang, T. Puzzer, T. Trupke, B. Richards, A. Shalav and K. Lin, *Thin Solid Films,* 2006, **511**, 654.
7 N.-M. Park, T.-S. Kim and S.-J. Park, *Appl. Phys. Lett.*, 2001, **78**, 2575.
8 B.-H. Kim, C.-H. Cho, J.-S. Mun, M.-K. Kwon, T.-Y. Park, J. S. Kim, C. C. Byeon, J. Lee and S.-J. Park, *Adv. Mater.*, 2008, **20**, 3100.
9 C.-H. Cheng, Y.-C. Lien, C.-L. Wu and G.-R. Lin, Opt. Express, 2013, **21**, 391.
10 L. Tsybeskov, K. D. Hirschman, S. P. Duttagupta, M. Zacharias, P. M. Fauchet, J. P. McCaffrey and D. J. Lockwood, *Appl. Phys. Lett.,* 1998, **72**, 43.
11 M. Zacharias, J. Heitmann, R. Scholz, U. Kahler, M. Schmidt and J. Bläsing, *Appl. Phys. Lett.*, 2002, **80**, 661.
12 B. Rezgui, A. Sibai, T. Nychyporuk, M. Lemiti, G. Bremond, D. Maestre and O. Palais, *Appl. Phys. Lett.,* 2010, **96**, 183105.
13 S. Jang, C. Ko, J. Joo, K. Jung, M. Han, E. Kim and K. Park, *J. Korean Phys. Soc.*, 2008, **53**, 1622.
14 S. Jang, S. Jung, E. Choi, M. Han and J. Lee, *J. Korean Phys. Soc.*, 2011, **59**, 2334.
15 M. V. Wolkin, J. Jorne, P. M. Fauchet, G. Allan and C. Delerue, *Phys. Rev. Lett.*, 1999, **82**, 197.
16 D. Hiller, M. Jivanescu, A. Stesmans and M. Zacharias, *J. Appl. Phys.,* 2010, **107**, 084309.
17 R. M. Van Ginhoven, H. Jónsson, K. A. Peterson, M. Dupuis and L. R. Corrales, *J. Chem. Phys.*, 2003, **118**, 6582.
18 A. N. Trukhin, M. Goldberg, J. Jansons, H.-J. Fitting, I. A. Tale, *J. Non-Cryst. Solids,* 1998, **223**, 114.
19 G.-R. Lin, C.-J. Lin and K.-C. Yu, *J. Appl. Phys.,* 2004, **96**, 3025.
20 D. Hiller, S. Goetze, F. Munnik, M. Jivanescu, J. W. Gerlach, J. Vogt, E. Pippel, N. Zakharov, A. Stesmans and M. Zacharias, *Phys. Rev. B*, 2010, **82**, 195401.
21 T. Li, F. Gygi and G. Galli, *Phys. Rev. Lett.*, 2011, **107**, 206805.
22 M. Dasog, G. B. De los Reyes, L. V. Titova, F. A. Hegmann and J. G. C. Veinot, *ACS Nano,* 2014, **8**, 9636.
23 M. Dasog, Z. Yang, S. Regli, T. M. Atkins, A. Faramus, M. P. Singh, E. Muthuswamy, S. M. Kauzlarich, R. D. Tilley and J. G. C. Veinot, *ACS Nano*, 2013, **7**, 2676.
24 W-K Hong, G. Jo, J. I. Sohn, W. Park, M. Choe, G. Wang, Y. H. Kahng, M. E. Welland and T. Lee, *ACS Nano*, 2009, **4**, 811.
25 Z. F. Di, Y. Q. Wang, M. Nastasi, G. Bisognin, M. Berti and P. E. Thompson, *Appl. Phys. Lett.*, 2009, **94**, 264102.
26 H.-Y. Kim, C. F. Lo, L. Liu, F. Ren, J. Kim and S. J. Pearton, *Appl. Phys. Lett.,* 2012, **100**, 012107.
27 S. Ismail-Beigi and S. G. Louie, *Phys. Rev. Lett.*, 2005, **95**, 156401.
28 M. A. Stevens Kalceff and M. R. Phillips, *Phys. Rev. B*, 1995, **52**, 3122.
29 C. Itoh, T. Suzuki and N. Itoh, *Phys. Rev. B*, 1990, **41**, 3794.
30 K. Tanimura, C. Itoh and N. Itoh, *J. Phys. C.*, 1988, **21**, 1869.
31 J. Heitmann, F. Müller, L. X. Yi, M. Zacharias, D. Kovalev and F. Eichhorn, *Phys. Rev. B*, 2004, **69**, 195309.
32 A. R. Wilkinson and R. G. Elliman, *Phys. Rev. B*, 2003, **68**, 155302.
33 J. Linnros, N. Lalic, A. Galeckas and V. Grivickas, *J. Appl. Phys.*, 1999, **86**, 6128.
34 L. Pavesi, *J. Appl. Phys.*, 1996, **80**, 216.
35 G. Kresse and J. Hafner, *Phys. Rev. B*, 1993, **47**, 558.
36 G. Kresse and J. Furthmüller, *Phys. Rev. B*, 1999, **54**, 11169.
37 J. P. Perdew, K. Burke and M. Ernzerhof, *Phys. Rev. Lett.*, 1996, **77**, 3865.
38 P. E. Blöchl, *Phys. Rev. B*, 1994, **50**, 17953.
39 S. Kim, J.-S. Park and K. J. Chang, *Nano Lett.*, 2012, **12**, 5068.
40 Q. Wang, B. Xu, J. Sun, H. Liu, Z. Zhao, D. Yu, C. Fan and J. He, *J. Am. Chem. Soc.*, 2014, **136**, 9826.
41 P. Zhang, X.D. Li, C.H. Hua, S.Q. Wu and Z.Z. Zhu, *Phys. Lett. A*, 2012, **376**, 1230.
42 K. Jarolimek, R. A. de Groot, G. A. de Wijs and M. Zeman, *Phys. Rev. B*, 2014, **90**, 125430.
43 Z. Zhou, L. Brus and R. Friesner, *Nano Lett.*, 2003, **3**, 163.
44 R. Guerra, E. Degoli and S. Ossicini, *Phys. Rev. B*, 2009, **80**, 155332.

Journal of Materials Chemistry C Accepted Manuscript

This journal is © The Royal Society of Chemistry 20xx